

Chaotic Roots of the Modular Multiplication Dynamical System in Shor’s Algorithm

Abu Musa Patoary,¹ Amit Vikram,¹ Laura Shou,² and Victor Galitski^{1,3}

¹*Joint Quantum Institute and Department of Physics,
University of Maryland, College Park, MD 20742, USA*

²*School of Mathematics, University of Minnesota, Minneapolis, MN 55455, USA*

³*Center for Computational Quantum Physics, The Flatiron Institute, New York, NY 10010, United States*

(Dated: June 30, 2023)

Shor’s factoring algorithm, believed to provide an exponential speedup over classical computation, relies on finding the period of an exactly periodic quantum modular multiplication operator. This exact periodicity is the hallmark of an integrable system, which is paradoxical from the viewpoint of quantum chaos, given that the classical limit of the modular multiplication operator is a highly chaotic system that occupies the “maximally random” Bernoulli level of the classical ergodic hierarchy. In this work, we approach this apparent paradox from a quantum dynamical systems viewpoint, and consider whether signatures of ergodicity and chaos may indeed be encoded in such an “integrable” quantization of a chaotic system. We show that Shor’s modular multiplication operator, in specific cases, can be written as a superposition of quantized A -baker’s maps exhibiting more typical signatures of quantum chaos and ergodicity. This work suggests that the integrability of Shor’s modular multiplication operator may stem from the interference of other “chaotic” quantizations of the same family of maps, and paves the way for deeper studies on the interplay of integrability, ergodicity and chaos in and via quantum algorithms.

Introduction — Shor’s algorithm [1, 2] to factorize an integer N is a cornerstone of quantum computation [3], being exponentially faster than all known classical factorization algorithms and capable of breaking RSA encryption [4], a widely used scheme for secure data transmission. Interestingly, the success of this algorithm hinges on a foundational tension with the very notion of “quantum chaos” [5]: the quantum modular multiplication operator at the core of Shor’s algorithm [1–3] belongs to a class of quantum systems that have a strongly chaotic classical limit, but violate several expected signatures of “chaos” on quantization.

The quantization of classically ergodic, chaotic systems [5, 6] is typically associated with spectral signatures such as non-degenerate energy levels and spectral rigidity, as supported by general theoretical arguments and numerical studies of several systems [5, 7–16]. Paradoxically, as indicated above, some quantizations [1, 17] of certain canonical textbook examples of classically ergodic and chaotic systems [6] – such as modular multiplication $f_A(x) = (Ax \bmod N)$ on a 1D interval $x \in [0, N)$ (quantized in Shor’s algorithm) and Arnold’s cat map on the torus — are *exactly periodic* at long times with highly degenerate and orderly spectra [1, 18], which is at odds with ergodic quantum dynamics [16]. This is because quantization itself is not a uniquely defined procedure, and several distinct quantum systems can have the same classical limit (e.g., Refs. [1, 19–21] consider entirely different quantizations of $f_2(x)$ with different spectral properties). In particular, the (conventionally) “standard” quantization of each of the above maps [1, 17] captures the dynamics of only a *measure-zero* subset of periodic orbits with a common (not necessarily fundamental) period [6, 22]. This gives the appearance of early-time “chaos” on quantization via the exponential divergence of typical nearby orbits, but completely misses out on the full ergodic and

chaotic classical dynamics at late times in the bulk of the phase space.

On the one hand, the example of Shor’s algorithm demonstrates a possibly generic need to eliminate “quantum chaos” in the quantization of even a classically chaotic map, for its successful utilization in certain quantum algorithms. On the other, it also suggests the more fundamental question of whether appropriate manifestations of quantum ergodicity and chaos can be hidden in some way even in such non-ergodic quantizations. Interestingly, a partial resolution to this question was noted in Refs. [23, 24], where it was shown [24] that the unitary operator implementing modular multiplication by $A = 2$ in Shor’s algorithm can be expressed as a superposition of quantized baker’s maps [20, 25], which may be regarded as “chaotic” quantizations of $f_2(x)$ [more precisely, of baker’s maps [6] in a 2D phase space (x, p) whose action on the position coordinate $x \in [0, 1)$ is identical to $f_2(Nx)/N$] that by and large exhibit the expected signatures of quantum chaos and ergodicity [20, 21].

In this work, we show that this “embedding” of a superposition of “quantum chaotic” maps in the periodic modular multiplication map generalizes to an arbitrary multiplier A . The appropriate chaotic maps are direct generalizations of the 2D A -baker’s maps (extensions of baker’s maps whose 1D projection is $f_A(Nx)/N$), and these maps can be quantized in terms of certain combinations of discrete Fourier transforms [20], when either $N+1$ or $N-1$ is a multiple of A . This establishes a rigorous correspondence between specific “ergodic” and “non-ergodic” quantizations of $f_A(x)$ for arbitrary A , which may serve as a simple model for understanding the interplay of integrability, ergodicity and chaos in different quantizations of the same system. We will now present the details of this correspondence, and subsequently discuss both its potential implications for studying the em-

bedding of quantum chaos in Shor’s algorithm, and in extending the quantization of A -baker’s maps to arbitrary N .

Results — In the remainder of this paper, we will refer to the exactly periodic quantum modular multiplication used in Shor’s algorithm simply as modular multiplication, without explicitly mentioning the qualifier “quantum”. Our main result (Eq. (8)) is to show that modular multiplication, in some specific cases, can be exactly written as a superposition of “chaotic” quantum A -baker’s maps. Modular multiplication U_A , given two co-primes N and A ($A < N$), is defined in an N dimensional Hilbert space according to the equation:

$$U_A |m\rangle = |mA \pmod{N}\rangle, \text{ for } m \in \{0, 1 \dots N-1\}, \quad (1)$$

where $\{|0\rangle, |1\rangle \dots |N-1\rangle\}$ forms an orthonormal basis. Since N and A are co-primes, modular multiplication is an exactly periodic unitary operator which permutes the basis states according to Eq. (1).

The classical A -baker’s map, a generalization of baker’s map, is a canonical example of an ergodic and chaotic system [26]. It maps a unit square to itself by stretching in one direction and compressing in the perpendicular direction in such a way that the total area of the square is preserved, and rearranging the stretched square to fit inside the unit square. The map is defined by the following transformation:

$$x \rightarrow x' = Ax - [Ax], \quad (2)$$

$$p \rightarrow p' = \frac{p + [Ax]}{A}. \quad (3)$$

Here $(x, p) \in [0, 1) \times [0, 1)$ are phase space coordinates and $[x]$ denotes the integer part of x . The map is illustrated in Fig. 1. The unit square is divided into A rectangles of equal area as shown in the left side of Fig. 1. Each of the rectangles is stretched by a factor of A along the horizontal direction and by $1/A$ along the vertical direction. Then the rectangles are stacked on top of each other as shown on the right side of Fig. 1. When

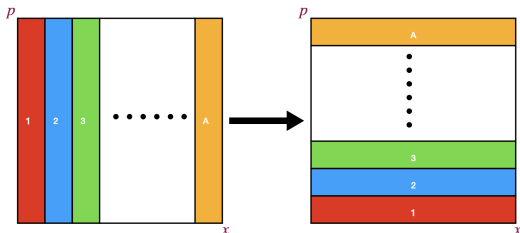


FIG. 1. The A -baker’s map transforms the unit square in the left to the one in the right. The unit square is divided into A rectangles which are marked by numbers from 1 to A . Each rectangle is stretched along x axis and contracted along p axis before being stacked on top of each other.

$A = 2$ the A -baker’s map reduces to the standard baker’s

map [27].

As with any classical dynamical system, there is no unique way to quantize the A -baker’s map. By convention, the basic requirements are that the quantum map is unitary and it reduces to the classical map in the semi-classical limit. Several quantization procedures satisfying these requirements have been developed for A -baker’s map [20, 21, 26, 28–30]. In this paper, we will use the quantization procedure developed by Balazs and Voros (BV)[20]. In BV quantization, one replaces the phase space of the classical map with a D dimensional Hilbert space. Then one can consider discrete position ($|x_n\rangle$) and momentum ($|p_n\rangle$) bases with the boundary conditions $|x_{n+D}\rangle = e^{-2\pi i\beta} |x_n\rangle$ and $|p_{n+D}\rangle = e^{2\pi i\alpha} |p_n\rangle$. Finally one constructs a $D \times D$ unitary matrix which transforms the states in ways analogous to the classical transformation in Eq. (2) and (3). This unitary matrix is the quantum A -baker’s map. The Hilbert space dimension D plays the role of \hbar^{-1} [20]. Therefore the semi-classical limit of this map is obtained by taking $D \rightarrow \infty$ which is equivalent to $\hbar \rightarrow 0$. We explain the associated procedures in detail in Sections I and III of the supplemental material. The quantum A -baker’s map, obtained using the BV procedure, is given by the following unitary matrix $B_A^{(0)}$:

$$B_A^{(0)} = (F_D^{\alpha,\beta})^{-1} \begin{bmatrix} F_D^{\alpha,\beta} & 0 & 0 & \dots & 0 \\ 0 & F_D^{\alpha,\beta} & 0 & \dots & 0 \\ 0 & 0 & F_D^{\alpha,\beta} & \dots & 0 \\ \vdots & \vdots & \vdots & \ddots & \vdots \\ 0 & 0 & 0 & \dots & F_D^{\alpha,\beta} \end{bmatrix}. \quad (4)$$

Here α, β are phases introduced in the boundary condition of position and momentum basis and $F_D^{\alpha,\beta}$ are generalized discrete Fourier transform (DFT) matrix whose elements are

$$[F_D^{\alpha,\beta}]_{nm} = \frac{1}{\sqrt{D}} e^{-2\pi i(n+\alpha)(m+\beta)/D}. \quad (5)$$

For periodic boundary conditions ($\alpha = \beta = 0$), $F_D^{\alpha,\beta}$ reduces to the standard DFT matrix. For notational convenience we will denote the standard DFT matrix simply by F_D . Note that D/A in Eq. (4) should be an integer which requires D to be a multiple of A .

One can modify the A -baker’s map so that the rectangles in the right side of Fig. 1 are stacked differently, and then use the same BV procedure to quantize this modified map. For example, if all the rectangles in the right side of Fig. 1 are cyclically permuted by one step so that now 1 goes to A , 2 goes to 1 ... 3 goes to 2, we get a different quantized map $B_A^{(1)}$. Similarly one can construct other quantum maps $B_A^{(2)}, B_A^{(3)} \dots B_A^{(A-1)}$ by cyclically permuting the horizontal rectangles by 2, 3, ..., $A-1$ steps respectively. The general equation for

the A -baker's map $B_A^{(k)}$ is

$$B_A^{(k)} = [F_D^{\alpha,\beta}]^{-1} \begin{bmatrix} 0 & \dots & k-1 & k & \dots & A-1 \\ 0 & \dots & 0 & F_{\frac{D}{A}}^{\alpha,\beta} & \dots & 0 \\ \vdots & \ddots & \vdots & \vdots & \ddots & \vdots \\ 0 & \dots & 0 & 0 & \dots & F_{\frac{D}{A}}^{\alpha,\beta} \\ F_{\frac{D}{A}}^{\alpha,\beta} & \dots & 0 & 0 & \dots & 0 \\ \vdots & \ddots & \vdots & \vdots & \ddots & \vdots \\ 0 & \dots & F_{\frac{D}{A}}^{\alpha,\beta} & 0 & \dots & 0 \end{bmatrix}, \quad (6)$$

where $k \in \{0, 1, \dots, A-1\}$. When $k=0$ it reduces to Eq. (4).

With this background we can state our main result. Given two co-prime integers N and A such that $N = Aq \pm 1$ where q is an integer, the corresponding modular multiplication operator U_A^\pm can be written to act instead on $D = Aq$ states (rather than on $N = Aq \pm 1$ as usual). This operator is obtained in the case $N = Aq + 1$ by removing the state $|0\rangle$ which is always a fixed point, $U_A^+|0\rangle = |0\rangle$, and in the case $N = Aq - 1$ by adding a D th state $|D-1\rangle$, with the extension $U_A^-|D-1\rangle = |D-1\rangle$ which agrees with the original map defined in Eq. (1). The modular multiplication map dynamics are thus preserved, but the advantage is the number of states is now a multiple of A . With these conventions, the $Aq \times Aq$ representation of the modular multiplication operator U_A^\pm can be expressed as

$$U_A^\pm = F_{Aq}^{-1} \begin{bmatrix} F_q & F_q^{0,\mp\frac{1}{A}} & F_q^{0,\mp\frac{2}{A}} & \dots & F_q^{0,\mp\frac{A-1}{A}} \\ F_q & F_q^{0,\mp\frac{1}{A}} & F_q^{0,\mp\frac{2}{A}} & \dots & F_q^{0,\mp\frac{A-1}{A}} \\ F_q & F_q^{0,\mp\frac{1}{A}} & F_q^{0,\mp\frac{2}{A}} & \dots & F_q^{0,\mp\frac{A-1}{A}} \\ \vdots & \vdots & \vdots & \vdots & \vdots \\ F_q & F_q^{0,\mp\frac{1}{A}} & F_q^{0,\mp\frac{2}{A}} & \dots & F_q^{0,\mp\frac{A-1}{A}} \end{bmatrix} \odot \tilde{F}_{Aq}^\mp. \quad (7)$$

Here \odot denotes Hadamard or entry-wise product of two matrices defined as $(A \odot B)_{ij} = A_{ij}B_{ij}$ and $\tilde{F}_{Aq}^\mp = F_A^\mp \otimes J_q$ with J_q being a $q \times q$ matrix with all elements equal to 1, F_A^+ the $A \times A$ DFT matrix with no phase, F_A^- the conjugate of F_A^+ and \otimes denoting tensor product. In Section II of the supplemental material we analytically derive Eq. (7).

To extract the quantized A -baker's maps embedded in Eq. (7), we rewrite it as:

$$U_A^\pm = \frac{1}{\sqrt{A}} \sum_{k=0}^{A-1} \tilde{B}_A^{\pm(k)}, \quad (8)$$

where $\tilde{B}_A^{\pm(k)}$ are quantized maps similar to the ones obtained in Eq. (6) but with some differences. Let us write

the explicit form of $\tilde{B}_A^{\pm(k)}$ to identify the differences:

$$\tilde{B}_A^{\pm(k)} = F_{Aq}^{-1} \begin{bmatrix} 0 & \dots & k-1 & k & \dots & A-1 \\ 0 & \dots & 0 & F_q^{0,\mp\frac{k}{A}} & \dots & 0 \\ \vdots & \ddots & \vdots & \vdots & \ddots & \vdots \\ 0 & \dots & 0 & 0 & \dots & F_q^{0,\mp\frac{A-1}{A}} \\ F_q & \dots & 0 & 0 & \dots & 0 \\ \vdots & \ddots & \vdots & \vdots & \ddots & \vdots \\ 0 & \dots & F_q^{0,\mp\frac{k-1}{A}} & 0 & \dots & 0 \end{bmatrix} \odot \tilde{F}_{Aq}^\mp. \quad (9)$$

Comparing Eq. (9) with Eq. (6) we notice two main differences: (i) In $\tilde{B}_A^{\pm(k)}$, the inverse of F_{Aq} has no phase and the phases of each $q \times q$ DFT matrices are different but in $B_A^{(k)}$ all of them have same phase, (ii) The Hadamard product in Eq. (9) is absent in Eq. (6). Despite these differences, the evolution of states under the operators $\tilde{B}_A^{\pm(k)}$ is very similar to that of $B_A^{(k)}$ in the semi-classical limit, and we will call $\tilde{B}_A^{\pm(k)}$ *quantum A-baker's maps*. We note that if we plot the matrix elements of $\tilde{B}_A^{\pm(k)}$ they resemble classical Bernoulli maps in the same way as the $B_A^{(k)}$ do (Fig. 2), although as we explain shortly this is not a sufficient criterion.

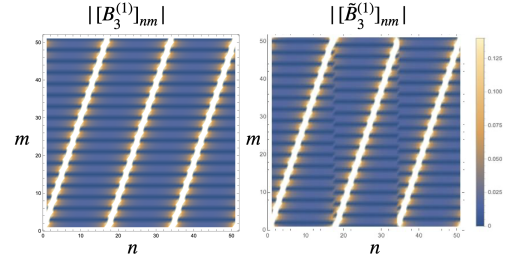


FIG. 2. The density plot of the absolute value of the matrix elements of $B_3^{(1)}$ (left) and $\tilde{B}_3^{(1)}$ (right) when $N = 52$. They are mostly identical except minor difference in the cuts between the 3 segments. Both of them resemble the classical A-baker's map for $A = 3$. This is necessary but not sufficient to claim that $\tilde{B}_3^{(1)}$ reduces to 3-baker's map in semi-classical limit.

Classical limit — To justify calling $\tilde{B}_A^{\pm(k)}$ a quantum A -baker's map, in Section III of the supplementary material we determine the action of $\tilde{B}_A^{\pm(k)}$ on Gaussian states (“coherent states”) maximally localized at a point (x, p) in phase space. We show that $\tilde{B}_A^{\pm(k)}$ sends such a state to another coherent state localized close to the classical evolution location $(Ax - \lfloor Ax \rfloor, \frac{p + (\lfloor Ax \rfloor - k) \bmod A}{A})$. We only do this for (x, p) away from the discontinuities of the classical A -baker map, otherwise there can be diffraction effects [28, 31, 32]. The action on coherent states can be interpreted in terms of the Wigner or Husimi function in phase space: A state whose Wigner/Husimi function is localized near (x, p) is transformed by $\tilde{B}_A^{\pm(k)}$

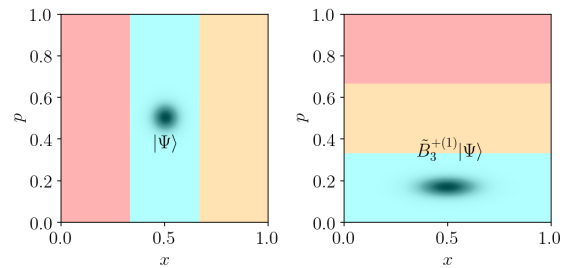
to a state localized near the classical trajectory point $(Ax - \lfloor Ax \rfloor, \frac{p + (\lfloor Ax \rfloor - k) \bmod A}{A})$. This correspondence between quantum and classical evolution is shown visually in Fig. 3.

Such an action on Gaussian states was used in [32] to prove a rigorous classical-quantum correspondence (Egorov-type theorem [32, Theorem 12]) for the original Balazs–Voros quantization of the baker map. In the case here, we will be content with just analyzing the behavior of $\tilde{B}_A^{\pm(k)}$ on Gaussian states. Due to the varying phases in the DFT matrices in Eq. (9), the action on Gaussian states will be more complicated than in the original Balazs–Voros quantization. In particular, the quantum evolved state here is actually centered a distance $\mathcal{O}_A(D^{-1})$ away from the classical trajectory point, though this will still be close enough for our purposes to the Gaussian state actually centered at the classical trajectory.

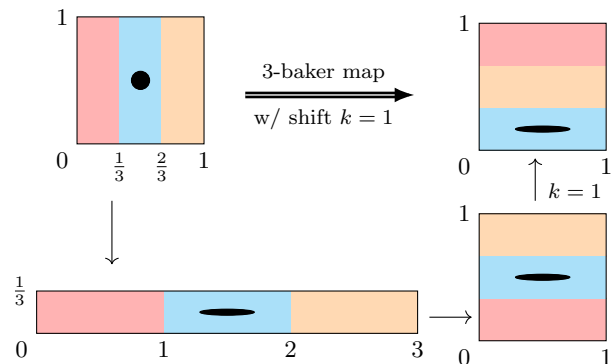
As noted previously, the matrix elements of $\tilde{B}_A^{\pm(k)}$ in the position basis (and momentum basis) trace out the classical 1D action of the position (momentum) coordinate in the A -baker map defined in Eqs. (2-3). This is not sufficient to conclude that $\tilde{B}_A^{\pm(k)}$ has the correct semiclassical behavior, as the Walsh baker quantizations considered in [26] also display this behavior, but as shown in [33] are not quantizations of the baker map. Instead the semi-classical limit there has to be interpreted as a “stochastic” or “multi-valued” baker map. One explanation for this is that even if the maps look classically correct in pure position or pure momentum basis, they may not entwine position and momentum together correctly. Thus checking the behavior in phase space, on coherent states or through Wigner/Husimi functions, is necessary to understand the semiclassical limit.

Discussion — We have illustrated a specific “embedding” of quantum chaotic behavior in the periodic orbits of a classically ergodic, chaotic map via quantum superposition, by deriving an exact correspondence between the periodic modular-multiplication-by- A maps and “chaotic” A -baker’s maps, for N such that either of $N \pm 1$ is a multiple of A . As will be shown in an upcoming work, this result generalizes to other values of N albeit via a more complicated construction with two important implications.

Firstly, in any practical implementation of Shor’s algorithm, it is N that is given while A is chosen as per convenience, in contrast to the dynamical systems approach, in which a fixed A specifies the modular multiplication map while $N \rightarrow \infty$ through any subsequence of \mathbb{N} gives the classical limit. This means that a general result for N would be crucial if one is to understand the implications of this “embedding of quantum chaos” for Shor’s algorithm (otherwise, choosing an A that is a factor of either of $N \pm 1$ would require the output of Shor’s algorithm as applied to $N \pm 1$, introducing a circular element). Conversely, achieving such a generalization may provide a fuller picture of how certain perturbations af-



(a) Phase space plots (Husimi functions) of the quantum evolution of a Gaussian state $|\Psi\rangle$ by $\tilde{B}_3^{+(1)}$, for $D = 150$. The state $|\Psi\rangle$ is localized at $(x, p) = (\frac{1}{2}, \frac{1}{2})$, and its time evolved state $\tilde{B}_3^{+(1)}|\Psi\rangle$ is localized near the classical trajectory point $(3x, \frac{p + (\lfloor Ax \rfloor - 1) \bmod A}{A}) = (\frac{1}{2}, \frac{1}{6})$. The colored rectangles are overlaid for easier comparison to the classical map in (b).



(b) Classical evolution of the unit square by the 3-baker map with cyclic shift $k = 1$, which sends $(x, p) \mapsto (3x - \lfloor 3x \rfloor, \frac{p + (\lfloor Ax \rfloor - 1) \bmod A}{A})$. The total classical transformation is shown in the top row, while the intermediate components of stretching, cutting and stacking, and cyclic permutation are shown through the two stages in the bottom row. The action on a disk is also shown for comparison to part (a).

FIG. 3. Comparison of the quantum evolution under $\tilde{B}_3^{+(1)}$, and the classical evolution by the 3-baker map with cyclic shift $k = 1$. The time-evolved quantum state $\tilde{B}_3^{+(1)}|\Psi\rangle$ shown in (a) follows the classical action shown in (b), and also displays the stretching in x -direction and shrinking in p -direction characteristic of the classical A -baker map.

fect the dynamics of Shor’s algorithm, along the lines of the analysis in Ref. [24].

Secondly, from a fundamental quantum dynamical systems viewpoint, the study of quantized A -baker’s maps has generally been restricted to Hilbert space dimensions that are multiples of A , due to a need to consider A copies of discrete Fourier transforms in, e.g., the Balazs–Voros quantization [20]. Approaching the quantization of such maps through the above connection to Shor’s algorithm, on the other hand, provides a promising avenue to generalize A -baker’s maps to a wider set of Hilbert space dimensions (or choices of N) with the use of *generalizations* of Fourier transforms, in particular for any coprime pair of (A, N) . This also opens avenues for studying the semi-

classical behavior of such generalized quantum A -baker's maps to explore atypicalities and any N -dependence in their "quantum chaos" signatures, noting that such atypicalities were observed for N a multiple of A in the Balazs-Voros quantization [20]. Further, A -baker's maps can be directly realized in quantum simulators using quantum Fourier transforms [34, 35], which may allow the experimental detection of such atypical spectral signatures using recently developed measurement protocols

for signatures of "quantum chaos" [36, 37].

Acknowledgments – This work was primarily supported by the U.S. Department of Energy, Office of Science, Basic Energy Sciences under Award No. DE-SC0001911 (V.G. and A.V., theory of quantum chaos). A.P. (establishing a connection between quantum maps and Shor's algorithm) acknowledges support from the National Science Foundation (QLCI grant OMA-2120757). L.S. was supported by Simons Foundation grant 563916, SM.

-
- [1] P. W. Shor, Algorithms for quantum computation: discrete logarithms and factoring, in *Proceedings 35th annual symposium on foundations of computer science* (IEEE, 1994) pp. 124–134.
- [2] P. W. Shor, Polynomial-time algorithms for prime factorization and discrete logarithms on a quantum computer, *SIAM review* **41**, 303 (1999).
- [3] M. A. Nielsen and I. L. Chuang, *Quantum Computation and Quantum Information* (Cambridge University Press, 2010).
- [4] R. L. Rivest, A. Shamir, and L. Adleman, A method for obtaining digital signatures and public-key cryptosystems, *Communications of the ACM* **21**, 120 (1978).
- [5] F. Haake, *Quantum signatures of chaos* (Springer, Berlin, Heidelberg, 2001).
- [6] E. Ott, *Chaos in dynamical systems* (Cambridge University Press, 2002).
- [7] S. W. McDonald and A. N. Kaufman, Spectrum and eigenfunctions for a Hamiltonian with stochastic trajectories, *Phys. Rev. Lett.* **42**, 1189 (1979).
- [8] G. Casati, F. Valz-Gris, and I. Guarnieri, On the connection between quantization of nonintegrable systems and statistical theory of spectra, *Lett. Nuovo Cimento* **28**, 279 (1980).
- [9] M. V. Berry, Quantizing a classically ergodic system: Sinai's billiard and the KKR method, *Ann. Phys.* **131**, 163 (1981).
- [10] O. Bohigas, M.-J. Giannoni, and C. Schmit, Characterization of chaotic quantum spectra and universality of level fluctuation laws, *Phys. Rev. Lett.* **52**, 1 (1984).
- [11] J. H. Hannay and A. M. Ozorio de Almeida, Periodic orbits and a correlation function for the semiclassical density of states, *J. Phys. A: Math. Gen.* **17**, 3429 (1984).
- [12] M. V. Berry, Semiclassical theory of spectral rigidity, *Proc. Roy. Soc. Lond. A* **400**, 229 (1985).
- [13] N. Argaman, Y. Imry, and U. Smilansky, Semiclassical analysis of spectral correlations in mesoscopic systems, *Phys. Rev. B* **47**, 4440 (1993).
- [14] S. Müller, S. Heusler, P. Braun, F. Haake, and A. Altland, Semiclassical foundation of universality in quantum chaos, *Phys. Rev. Lett.* **93**, 014103 (2004).
- [15] S. Müller, S. Heusler, P. Braun, F. Haake, and A. Altland, Periodic-orbit theory of universality in quantum chaos, *Phys. Rev. E* **72**, 046207 (2005).
- [16] A. Vikram and V. Galitski, Dynamical quantum ergodicity from energy level statistics, *arXiv preprint arXiv:2205.05704* (2022).
- [17] J. Hannay and M. V. Berry, Quantization of linear maps on a torus-fresnel diffraction by a periodic grating, *Phys. D: Nonlinear Phenom.* **1**, 267 (1980).
- [18] J. P. Keating, The cat maps: quantum mechanics and classical motion, *Nonlinearity* **4**, 309 (1991).
- [19] P. Pakoński, K. Życzkowski, and M. Kuś, Classical 1D maps, quantum graphs and ensembles of unitary matrices, *J. Phys. A: Math. Gen.* **34**, 9303 (2001).
- [20] N. L. Balazs and A. Voros, The quantized baker's transformation, *Ann. Phys.* **190**, 1 (1989).
- [21] M. Saraceno, Classical structures in the quantized baker transformation, *Ann. Phys.* **199**, 37 (1990).
- [22] F. J. Dyson and H. Falk, Period of a discrete cat mapping, *The American Mathematical Monthly* **99**, 603 (1992).
- [23] A. Lakshminarayan, Shuffling cards, factoring numbers and the quantum baker's map, *J. Phys. A: Math. Gen.* **38**, L597 (2005).
- [24] A. Lakshminarayan, Modular multiplication operator and quantized baker's maps, *Phys. Rev. A* **76**, 042330 (2007).
- [25] N. Balazs and A. Voros, The quantized baker's transformation, *Europhysics Letters* **4**, 1089 (1987).
- [26] N. Anantharaman and S. Nonnenmacher, Entropy of semiclassical measures of the Walsh-quantized baker's map, *Ann. Henri Poincaré* **8**, 37 (2007).
- [27] A. Rényi, Representations for real numbers and their ergodic properties, *Acta Math. Acad. Sci. Hungar* **8**, 477 (1957).
- [28] M. Saraceno and A. Voros, Towards a semiclassical theory of the quantum baker's map, *Phys. D: Nonlinear Phenom.* **79**, 206 (1994).
- [29] R. Rubin and N. Salwen, A canonical quantization of the baker's map, *Ann. Phys.* **269**, 159 (1998).
- [30] L. Ermann and M. Saraceno, Generalized quantum baker maps as perturbations of a simple kernel, *Phys. Rev. E* **74**, 046205 (2006).
- [31] S. De Bièvre and M. Degli Esposti, Egorov theorems and equidistribution of eigenfunctions for the quantized sawtooth and baker maps, *Ann. Inst. H. Poincaré Phys. Théor.* **69**, 1 (1998).
- [32] M. Degli Esposti, S. Nonnenmacher, and B. Winn, Quantum variance and ergodicity for the baker's map, *Comm. Math. Phys.* **263**, 325 (2006).
- [33] M. M. Tracy and A. J. Scott, The classical limit for a class of quantum baker's maps, *J. Phys. A* **35**, 8341 (2002).
- [34] T. A. Brun and R. Schack, Realizing the quantum baker's map on a NMR quantum computer, *Phys. Rev. A* **59**, 2649 (1999).
- [35] Y. S. Weinstein, S. Lloyd, J. Emerson, and D. G. Cory, Experimental implementation of the quantum baker's map, *Phys. Rev. Lett.* **89**, 157902 (2002).
- [36] D. V. Vasilyev, A. Grankin, M. A. Baranov, L. M. Sieberer, and P. Zoller, Monitoring quantum simulators

via quantum nondemolition couplings to atomic clock qubits, *PRX Quantum* **1**, 020302 (2020).

[37] L. K. Joshi, A. Elben, A. Vikram, B. Vermersch, V. Galitski, and P. Zoller, Probing many-body quantum chaos

with quantum simulators, *Phys. Rev. X* **12**, 011018 (2022).

[38] A. Bouzouina and S. De Bièvre, Equipartition of the eigenfunctions of quantized ergodic maps on the torus, *Comm. Math. Phys.* **178**, 83 (1996).

Supplementary Material for “Chaotic Roots of the Modular Multiplication Dynamical System in Shor’s Algorithm”

I. QUANTIZATION OF THE A-BAKER’S MAP

In this section, we will explain the quantization procedure of the A-baker’s map based on the work by Balazs and Voros [20]. Classically A-baker’s map transforms a unit square phase space onto itself according to the following equations:

$$x \rightarrow x' = Ax - [Ax], \quad (\text{S1})$$

$$p \rightarrow p' = \frac{p + [Ax]}{A}. \quad (\text{S2})$$

Here x and p are two variables of phase space and A is an integer. There is a simple pictorial representation of the map

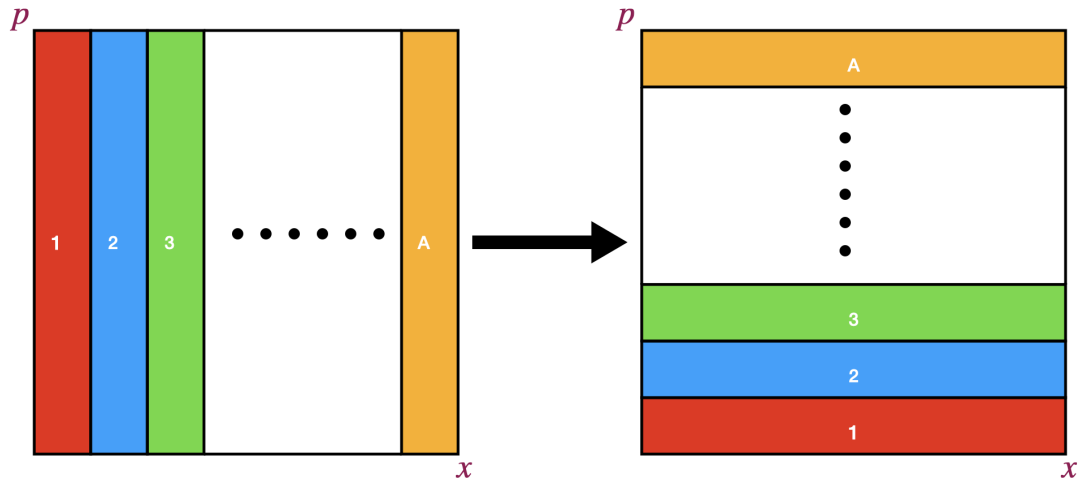


FIG. S1. A-baker’s map transforms the unit square in the left to the one in the right. The unit square is divided into A rectangles which are marked by numbers from 1 to A . Each rectangle is stretched along x axis and contracted along p axis before being stacked on top of each other.

which is shown in Fig. S1. First divide the unit square into A rectangles. Then stretch each rectangles in horizontal direction and contracts in vertical direction and finally stack the rectangles on top of each other. To quantize this map, instead of a phase space we consider a D dimensional Hilbert space. Suppose $\{|x_n\rangle\}_{n=0}^{D-1}$ and $\{|p_m\rangle\}_{m=0}^{D-1}$ are two different complete basis. We assume that they satisfy the following boundary conditions:

$$|x_{n+D}\rangle = e^{-2\pi i\beta} |x_n\rangle, \quad (\text{S3})$$

$$|p_{n+D}\rangle = e^{2\pi i\alpha} |p_n\rangle. \quad (\text{S4})$$

When $\alpha = \beta = 0$ it becomes periodic boundary condition. Physically one can think of these two basis as the eigenbasis of discrete position and momentum operator. The inner product of them is

$$\langle p_m | x_n \rangle = \frac{1}{\sqrt{D}} e^{-\frac{2\pi i(n+\alpha)(m+\beta)}{D}} = [F_D^{\alpha,\beta}]_{nm}, \quad (\text{S5})$$

where $F_D^{\alpha,\beta}$ is a $D \times D$ DFT matrix with phase α and β . Let's look at an arbitrary state $|\psi\rangle$ in the Hilbert space. We write the state as

$$\begin{aligned} |\psi\rangle &= \sum_{n=0}^{D-1} |x_n\rangle \langle x_n | \psi \rangle \\ &= \sum_{n=0}^{\frac{D}{A}-1} |x_n\rangle \langle x_n | \psi \rangle + \sum_{n=\frac{D}{A}}^{\frac{2D}{A}-1} |x_n\rangle \langle x_n | \psi \rangle \cdots \sum_{n=\frac{D(A-1)}{A}}^{D-1} |x_n\rangle \langle x_n | \psi \rangle \\ &= \sum_{l=1}^A |\psi_l\rangle, \end{aligned} \quad (\text{S6})$$

where $|\psi_l\rangle = \sum_{n=\frac{D(l-1)}{A}}^{\frac{Dl}{A}-1} |x_n\rangle \langle x_n | \psi \rangle$. Essentially we have partitioned the state in such a way that the projection of each partition into position basis can have non-zero value only inside a region. The regions are obtained from the equation

$$\langle x_n | \psi_l \rangle = 0 \quad \text{for} \quad 0 \leq n \leq \frac{D(l-1)}{A} - 1 \quad \text{and} \quad \frac{Dl}{A} \leq n \leq D-1. \quad (\text{S7})$$

The quantized A-baker's map is the unitary operator $B_A^{(0)}$ such that

$$B_A^{(0)} |\psi_l\rangle = |\phi_l\rangle \quad \text{for} \quad l = 1, 2, \dots, A. \quad (\text{S8})$$

Eq. (S8) implies that $B_A^{(0)} |\psi\rangle = \sum_{l=1}^A |\phi_l\rangle \equiv |\phi\rangle$. The states $|\phi_l\rangle$ are defined in a similar way as Eq. (S6) but in momentum basis i.e. $|\phi_l\rangle = \sum_{n=\frac{D(l-1)}{A}}^{\frac{Dl}{A}-1} |p_n\rangle \langle p_n | \phi \rangle$. Furthermore $|\phi_l\rangle$ satisfies

$$\langle x_{An} | \phi_l \rangle = \frac{1}{\sqrt{A}} \langle x_n | \psi_l \rangle \quad \text{for} \quad \frac{D(l-1)}{A} \leq n \leq \frac{Dl}{A} - 1, \quad (\text{S9})$$

$$\langle p_n | \phi_l \rangle = \sqrt{A} \langle p_{An} | \psi_l \rangle \quad \text{for} \quad \frac{D(l-1)}{A} \leq n \leq \frac{Dl}{A} - 1. \quad (\text{S10})$$

Eqs. (S9) and (S10) are analogous to expansion and contraction in the classical map. We insert a resolution of identity in Eq. (S10) and use the inner product of $|x_n\rangle$ and $|p_m\rangle$ to write

$$\begin{aligned} \langle p_n | \phi_l \rangle &= \sqrt{A} \sum_{m=0}^{D-1} \langle p_{An} | x_m \rangle \langle x_m | \psi_l \rangle \quad \text{for} \quad \frac{D(l-1)}{A} \leq n \leq \frac{Dl}{A} - 1 \\ &= \sqrt{\frac{A}{D}} \sum_{m=0}^{D-1} e^{-\frac{2\pi i A(n+\alpha)(m+\beta)}{D}} \langle x_m | \psi_l \rangle \\ &= \sum_{m=\frac{D(l-1)}{A}}^{\frac{Dl}{A}-1} (F_D^{\alpha,\beta})_{nm} \langle x_m | \psi_l \rangle. \quad [\text{using Eq. (S7)}] \end{aligned} \quad (\text{S11})$$

Note that $|\phi_l\rangle$ is defined in such a way that $\langle p_n | \phi_l \rangle$ when $\frac{D(l-1)}{A} \leq n \leq \frac{Dl}{A} - 1$ and $\frac{Dl}{A} \leq n \leq D-1$. Combining it with Eq. (S11) we get a relation between $|\phi_l\rangle$ and $|\psi_l\rangle$. However, in Eq. (S11) they are in different representation. One can show that $\langle p_n | \phi_l \rangle = \sum_{m=0}^{D-1} (F_D^{\alpha,\beta})_{mn} \langle x_m | \phi_l \rangle$. Consequently we can rewrite Eq. (S11) as

$$\langle x_n | \phi_l \rangle = \sum_{k=0}^{D-1} \sum_{m=\frac{D(l-1)}{A}}^{\frac{Dl}{A}-1} (F_D^{\alpha,\beta})_{nk}^{-1} (F_D^{\alpha,\beta})_{km} \langle x_m | \psi_l \rangle. \quad (\text{S12})$$

We compare Eq. (S12) with Eq. (S8) to get an expression for quantized A-baker's map $B_A^{(0)}$:

$$B_A^{(0)} = (F_D^{\alpha,\beta})^{-1} \begin{bmatrix} F_{\frac{D}{A}}^{\alpha,\beta} & 0 & 0 & \dots & 0 \\ 0 & F_{\frac{D}{A}}^{\alpha,\beta} & 0 & \dots & 0 \\ 0 & 0 & F_{\frac{D}{A}}^{\alpha,\beta} & \dots & 0 \\ \vdots & \vdots & \vdots & \ddots & \vdots \\ 0 & 0 & 0 & \dots & F_{\frac{D}{A}}^{\alpha,\beta} \end{bmatrix}. \quad (\text{S13})$$

We have derived the matrix form of B_A^0 without using Eq. (S9). But one can check that $B_A^{(0)}$ is consistent with Eq. (S9).

II. ANALYTICAL DERIVATION OF THE RELATION BETWEEN MODULAR MULTIPLICATION AND THE A-BAKER'S MAP

In this section we will derive Eq. (8) of the main paper. According to this equation, if N and A are two co-primes such that $N = qA \pm 1$ then modular multiplication matrix U_A^\pm satisfies

$$U_A^\pm = F_{Aq}^{-1} \begin{bmatrix} F_q & F_q^{0,\mp\frac{1}{A}} & F_q^{0,\mp\frac{2}{A}} & \dots & F_q^{0,\mp\frac{A-1}{A}} \\ F_q & F_q^{0,\mp\frac{1}{A}} & F_q^{0,\mp\frac{2}{A}} & \dots & F_q^{0,\mp\frac{A-1}{A}} \\ F_q & F_q^{0,\mp\frac{1}{A}} & F_q^{0,\mp\frac{2}{A}} & \dots & F_q^{0,\mp\frac{A-1}{A}} \\ \vdots & \vdots & \vdots & \vdots & \vdots \\ F_q & F_q^{0,\mp\frac{1}{A}} & F_q^{0,\mp\frac{2}{A}} & \dots & F_q^{0,\mp\frac{A-1}{A}} \end{bmatrix} \odot [F_A^\mp \otimes J_q]. \quad (\text{S14})$$

Here J_q is a $q \times q$ matrix whose all elements are 1, F_A is the $A \times A$ DFT matrix with no phase, \otimes denotes tensor product and \odot denotes Hadamard or entry-wise product of two matrices defined as $(A \odot B)_{ij} = A_{ij}B_{ij}$. The derivation is slightly different for two cases of $N = qA \pm 1$. We will do the calculation for $N = qA + 1$ and point out the differences with $N = qA - 1$ case. The modular multiplication is defined as

$$U_A |m\rangle = |mA \pmod{N}\rangle \text{ for } m = 0, 1, \dots, N-1. \quad (\text{S15})$$

From the definition one can see that the state $|0\rangle$ is always a fixed point of the modular multiplication. When $N = qA + 1$ we remove the $|0\rangle$ state such that the number of remaining states is a multiple of A . We denote this operator of dimension $Aq \times Aq$ as U^+ . Using Eq. (S15) we find that

$$\langle n|U_A^+|m\rangle = \delta_{n,Am-lN} \text{ for } lq+1 \leq m \leq (l+1)q \text{ and } l = 0, 1, \dots, A-1. \quad (\text{S16})$$

Here $\delta_{n,m}$ denotes Kronecker delta function. Since we have removed the $|0\rangle$ state all the blocks with same l have the same size. The Kronecker delta function can be written as

$$\begin{aligned} \delta_{n,Am-lN} &= \frac{1}{Aq} \sum_{k=1}^{Aq} e^{\frac{2\pi ik(n-Am+lN)}{Aq}} \\ &= \frac{1}{Aq} \sum_{k=1}^{Aq} e^{\frac{2\pi ikn}{Aq}} e^{\frac{-2\pi ik(m-\frac{l}{A})}{q}} \\ &= \frac{1}{Aq} \left[\sum_{k=1}^q e^{\frac{2\pi ikn}{Aq}} e^{\frac{-2\pi ik(m-\frac{l}{A})}{q}} + \sum_{k=q+1}^{2q} e^{\frac{2\pi ikn}{Aq}} e^{\frac{-2\pi ik(m-\frac{l}{A})}{q}} \dots + \sum_{k=(A-1)q+1}^{Aq} e^{\frac{2\pi ikn}{Aq}} e^{\frac{-2\pi ik(m-\frac{l}{A})}{q}} \right] \\ &= \frac{1}{Aq} \left[\sum_{k=1}^q e^{\frac{2\pi ikn}{Aq}} e^{\frac{-2\pi ik(m-\frac{l}{A})}{q}} + \sum_{k=1}^q e^{\frac{2\pi i(k+q)n}{Aq}} e^{\frac{-2\pi ik(m-\frac{l}{A})}{q}} e^{\frac{-2\pi il}{A}} \dots + \sum_{k=1}^q e^{\frac{2\pi i[k+(A-1)q]n}{Aq}} e^{\frac{-2\pi ik(m-\frac{l}{A})}{q}} e^{\frac{-2\pi il(A-1)}{A}} \right] \\ &= \frac{1}{\sqrt{A}} \sum_{k=1}^q [(F_{Aq})_{nk}^{-1} (F_q^{0,-\frac{l}{A}})_{km} + (F_{Aq})_{n(k+q)}^{-1} \omega_A^l (F_q^{0,-\frac{l}{A}})_{km} \dots + (F_{Aq})_{n[k+(A-1)q]}^{-1} \omega_A^{l(A-1)} (F_q^{0,-\frac{l}{A}})_{km}]. \end{aligned} \quad (\text{S17})$$

Here $\omega_A = e^{\frac{2\pi i}{A}}$ is the A^{th} root of unity. We have expressed the elements of modular multiplication in terms of DFT matrices. Using Eq. (S17) we can write modular multiplication as

$$U_A^+ = \frac{1}{\sqrt{A}} F_{Aq}^{-1} \begin{bmatrix} F_q & F_q^{0, -\frac{1}{A}} & F_q^{0, -\frac{2}{A}} & \dots & F_q^{0, -\frac{A-1}{A}} \\ F_q & \omega_A^1 F_q^{0, -\frac{1}{A}} & \omega_A^2 F_q^{0, -\frac{2}{A}} & \dots & \omega_A^{A-1} F_q^{0, -\frac{A-1}{A}} \\ F_q & \omega_A^2 F_q^{0, -\frac{1}{A}} & \omega_A^4 F_q^{0, -\frac{2}{A}} & \dots & \omega_A^{2(A-1)} F_q^{0, -\frac{A-1}{A}} \\ \vdots & \vdots & \vdots & \vdots & \vdots \\ F_q & \omega_A^{A-1} F_q^{0, -\frac{1}{A}} & \omega_A^{2(A-1)} F_q^{0, -\frac{2}{A}} & \dots & \omega_A^{(A-1)^2} F_q^{0, -\frac{A-1}{A}} \end{bmatrix}. \quad (\text{S18})$$

We can utilize Hadamard product to rewrite Eq. (S18) as

$$\begin{aligned} U_A^+ &= F_{Aq}^{-1} \begin{bmatrix} F_q & F_q^{0, -\frac{1}{A}} & F_q^{0, -\frac{2}{A}} & \dots & F_q^{0, -\frac{A-1}{A}} \\ F_q & F_q^{0, -\frac{1}{A}} & F_q^{0, -\frac{2}{A}} & \dots & F_q^{0, -\frac{A-1}{A}} \\ F_q & F_q^{0, -\frac{1}{A}} & F_q^{0, -\frac{2}{A}} & \dots & F_q^{0, -\frac{A-1}{A}} \\ \vdots & \vdots & \vdots & \vdots & \vdots \\ F_q & F_q^{0, -\frac{1}{A}} & F_q^{0, -\frac{2}{A}} & \dots & F_q^{0, -\frac{A-1}{A}} \end{bmatrix} \odot \frac{1}{\sqrt{A}} \begin{bmatrix} \omega_A^0 & \omega_A^0 & \omega_A^0 & \dots & \omega_A^0 \\ \omega_A^0 & \omega_A & \omega_A^2 & \dots & \omega_A^{A-1} \\ \omega_A^0 & \omega_A & \omega_A^4 & \dots & \omega_A^{2(A-1)} \\ \vdots & \vdots & \vdots & \vdots & \vdots \\ \omega_A^0 & \omega_A^{A-1} & \omega_A^{2(A-1)} & \dots & \omega_A^{(A-1)^2} \end{bmatrix} \otimes J_q \\ &= F_{Aq}^{-1} \begin{bmatrix} F_q & F_q^{0, -\frac{1}{A}} & F_q^{0, -\frac{2}{A}} & \dots & F_q^{0, -\frac{A-1}{A}} \\ F_q & F_q^{0, -\frac{1}{A}} & F_q^{0, -\frac{2}{A}} & \dots & F_q^{0, -\frac{A-1}{A}} \\ F_q & F_q^{0, -\frac{1}{A}} & F_q^{0, -\frac{2}{A}} & \dots & F_q^{0, -\frac{A-1}{A}} \\ \vdots & \vdots & \vdots & \vdots & \vdots \\ F_q & F_q^{0, -\frac{1}{A}} & F_q^{0, -\frac{2}{A}} & \dots & F_q^{0, -\frac{A-1}{A}} \end{bmatrix} \odot [F_A^{-1} \otimes J_q]. \end{aligned} \quad (\text{S19})$$

When $N = Aq - 1$ we add the state $|N\rangle$, which is a fixed state, so that the total number of states is a multiple of A . After adding the extra state we denote the operator as U^- and perform a similar calculation as above to find

$$U_A^- = F_{Aq}^{-1} \begin{bmatrix} F_q & F_q^{0, \frac{1}{A}} & F_q^{0, \frac{2}{A}} & \dots & F_q^{0, \frac{A-1}{A}} \\ F_q & F_q^{0, \frac{1}{A}} & F_q^{0, \frac{2}{A}} & \dots & F_q^{0, \frac{A-1}{A}} \\ F_q & F_q^{0, \frac{1}{A}} & F_q^{0, \frac{2}{A}} & \dots & F_q^{0, \frac{A-1}{A}} \\ \vdots & \vdots & \vdots & \vdots & \vdots \\ F_q & F_q^{0, \frac{1}{A}} & F_q^{0, \frac{2}{A}} & \dots & F_q^{0, \frac{A-1}{A}} \end{bmatrix} \odot [F_A \otimes J_q]. \quad (\text{S20})$$

III. SEMICLASSICAL LIMIT

In this section we consider the action of the matrices $\tilde{B}_A^{\pm(k)}$ defined in Eq. (9) on states in the semiclassical limit $D \rightarrow \infty$. For $\mathbf{z}_0 = (x_0, p_0)$ in the torus $\mathbb{T}^2 = \mathbb{R}^2/\mathbb{Z}^2$ (which we identify with the square $[0, 1) \times [0, 1)$) away from the discontinuities of the classical A -baker map, we will show that $\tilde{B}_A^{\pm(k)}$ evolves a Gaussian state localized at \mathbf{z}_0 to one localized close to the classical evolution value $S_A^{(k)}(\mathbf{z}_0) := (Ax - \lfloor Ax \rfloor, \frac{p + (\lfloor Ax \rfloor - k) \bmod A}{A})$. For this reason we refer to the matrices $\tilde{B}_A^{\pm(k)}$ as a quantum version of the classical A -baker map (with a cyclic k -shift). We note that due to the phases α_j, β_j , the quantum evolved state is actually centered at a point $S_A^{(k)}(\mathbf{z}_0) + \mathcal{O}_A(D^{-1})$, but this will end up being sufficiently close to the state centered at $S_A^{(k)}(\mathbf{z}_0)$ in the limit $D \rightarrow \infty$ for our purposes here. This error slows down the rate of convergence as $D \rightarrow \infty$ however.

In this section, D is the dimension of the matrices, and we will allow A to grow with the dimension D as long as $A = o(D^{1/2}(\log D)^{-1/2})$. The computations here will be very similar to those in [32, Prop. 5], though the addition of the phases α and β in the generalized DFT matrices will require some additional consideration, e.g. Eq. (S27).

Besides cyclic shifts by k elements, we will allow any permutation of blocks in $\tilde{B}_A^{\pm(0)}$ in Eq. (9). To this end, let $\Pi : \{0, \dots, A-1\} \rightarrow \{0, \dots, A-1\}$ be a permutation on A elements, and let P_Π be the $A \times A$ permutation matrix corresponding to Π . To make this permutation act on blocks, define the $D \times D$ matrix $P_{D, \Pi} := P_\Pi \otimes I_{D/A}$, where

$I_{D/A}$ is the $D/A \times D/A$ identity matrix. Then for $D \in \mathbb{A}\mathbb{N}$, define

$$\tilde{B}_A^{(\Pi)} := F_D^{-1} P_{D,\Pi} \begin{bmatrix} \omega_0 F_{D/A}^{\alpha_0, \beta_0} & 0 & \cdots & 0 \\ 0 & \omega_1 F_{D/A}^{\alpha_1, \beta_1} & \cdots & 0 \\ \vdots & & \ddots & \vdots \\ 0 & \cdots & 0 & \omega_{A-1} F_{D/A}^{\alpha_{A-1}, \beta_{A-1}} \end{bmatrix}, \quad (\text{S21})$$

where ω_j are arbitrary phase factors, $\alpha_j, \beta_j \in [-1, 1]$, and $P_{D,\Pi}$ acts by permuting row blocks on the block matrix to the right according to Π . In this notation, $\tilde{B}_A^{\pm(k)}$ from the main text corresponds to the special case of $\tilde{B}_A^{(\Pi)}$, where Π is the cyclic shift by k elements $\Pi^{(k)} : n \mapsto n - k \bmod A$, $\alpha_j = 0$, $\beta_j = \mp j/A$, and $\omega_j = e^{\pm 2\pi i j(j-k \bmod A)/D}$. For later use it will also be useful to define $\tilde{B}_A^{(\Pi)}$ in a mixed position-momentum basis,

$$\tilde{B}_{A,\text{mix}}^{(\Pi)} := F_D \tilde{B}_A^{(\Pi)}. \quad (\text{S22})$$

The associated classical map on the torus will be

$$S_A^{(\Pi)}(x, p) := \left(Ax - \lfloor Ax \rfloor, \frac{p + \Pi(\ell)}{A} \right), \quad \text{for } x \in \left[\frac{\ell}{A}, \frac{\ell+1}{A} \right), \ell = 0, \dots, A-1. \quad (\text{S23})$$

This is just the classical A -baker map with the permutation Π applied to the stacking of the blocks shown on the right side of Figure S1. Note that for $x \in [\frac{\ell}{A}, \frac{\ell+1}{A})$, that $\ell = \lfloor Ax \rfloor$.

A. Gaussian states on the torus

We work on the D -dimensional Hilbert space of periodic states. Usually one would associate $F_{D/A}^{\alpha_j, \beta_j}$ with the Hilbert space of *quasi*-periodic states corresponding to phase factors α, β , but since we work with several different α_j, β_j , there is no single particularly favored choice of phase conditions, and so we pick the periodic (no phase) boundary conditions for simplicity. We first consider the \mathbb{R}^2 -Gaussian state (also called ‘‘coherent state’’) localized at a point $\mathbf{z}_0 = (x_0, p_0) \in \mathbb{R}^2$ with squeezing parameter $\sigma > 0$,

$$\Psi_{\mathbf{z}_0, \sigma}(x) = (2D\sigma)^{1/4} e^{-\pi i D x_0 p_0} e^{2\pi i D p_0 x} e^{-\sigma D \pi (x-x_0)^2}, \quad x \in \mathbb{R}.$$

The corresponding torus coherent state $\Psi_{\mathbf{z}, \sigma, \mathbb{T}^2} \in \mathcal{C}^D$ is obtained by periodicizing the \mathbb{R}^2 -state in position and momentum, resulting in

$$\langle m | \Psi_{\mathbf{z}_0, \sigma, \mathbb{T}^2} \rangle = \sum_{v \in \mathbb{Z}} \Psi_{\mathbf{z}_0, \sigma} \left(\frac{m}{D} + v \right), \quad m \in \mathbb{Z}/D\mathbb{Z}. \quad (\text{S24})$$

For further details, see [32, 38].

The main properties we will use, in addition to the explicit formula for a Gaussian state, are the following.

1. For $0 < \delta < \frac{1}{2}$ and $x_0 \in (\delta, 1 - \delta)$, the torus coherent state $\Psi_{(x_0, p_0), \sigma, \mathbb{T}^2}$ is well-approximated by the \mathbb{R}^2 -coherent state $\Psi_{(x_0, p_0), \sigma}$: For $(\sigma D) \geq 1$ and $j = 0, \dots, D-1$,

$$\sqrt{D} \langle j | \Psi_{\mathbf{z}_0, \sigma, \mathbb{T}^2} \rangle = \Psi_{\mathbf{z}_0, \sigma} \left(\frac{j}{D} \right) + \mathcal{O}((\sigma D)^{1/4} e^{-\pi \sigma D \delta^2}), \quad (\text{S25})$$

with a uniform implied constant in the error term. This is due to the rapid decay of the \mathbb{R}^2 -Gaussian states, and is useful so we can apply the Gaussian transformation properties of the \mathbb{R}^2 -states,

$$\begin{aligned} \psi_{(x_0, p_0), \sigma}(x+s) &= \psi_{(x_0-s, p_0), \sigma}(x) e^{\pi i D p_0 s} \\ \psi_{(x_0, p_0), \sigma}(rx) &= \psi_{(x_0/r, p_0 r), r^2 \sigma}(x) \frac{1}{\sqrt{r}} \\ \psi_{(x_0, p_0), \sigma}(x) &= \psi_{(x_0, p_0+g), \sigma}(x) e^{i\pi D g x_0} e^{-2\pi i D g x}. \end{aligned}$$

2. The Fourier transform action on \mathbb{R}^2 -Gaussian states translates to the torus Gaussian states through the DFT matrix,

$$F_D \Psi_{\mathbf{z}_0, \sigma, \mathbb{T}^2} = \Psi_{F_{\mathbf{z}_0, 1/\sigma, \mathbb{T}^2}},$$

where $F_{\mathbf{z}_0} := (p_0, -x_0)$. We will have to show the generalized DFT matrices $F_D^{\alpha, \beta}$ act in a similar enough way in the semiclassical limit. For later use, we will use the following identity to relate $F_D^{\alpha, \beta}$ to F_D : For $j \in \{0, \dots, A-1\}$ and $m - jD/A, \xi - \ell D/A \in \{0, \dots, D/A - 1\}$,

$$\langle m - jD/A | F_D^{\alpha, \beta} | \xi - \ell D/A \rangle = \sqrt{A} \langle Am - jD | F_D | \xi \rangle e^{-2\pi i (\beta \frac{A}{D} m + \alpha \frac{A}{D} \xi - j\beta - \alpha \ell + \alpha \beta \frac{A}{D})}. \quad (\text{S26})$$

3. If $\mathbf{z}_0, \mathbf{z}_1 \in \mathbb{T}^2$ are close enough, then the coherent states centered at \mathbf{z}_0 and \mathbf{z}_1 are close up to an overall phase factor: If $\eta, \varepsilon = o(D^{-1/2})$ and $\sigma > 0$ is fixed, then for $x_0 \in (\delta, 1 - \delta)$ with $\delta \gg D^{-1/2}(\log D)^{-1/2}$, there is a phase factor $e^{i\Theta_{D, \eta, \varepsilon, \mathbf{z}_0}}$ so that

$$\left\| \Psi_{(x_0, p_0), \sigma, \mathbb{T}^2} - e^{i\Theta_{D, \eta, \varepsilon, \mathbf{z}_0}} \Psi_{(x_0 + \eta, p_0 + \varepsilon), \sigma, \mathbb{T}^2} \right\| = o(1), \quad \text{as } D \rightarrow \infty. \quad (\text{S27})$$

One can check this by estimating the euclidean norm directly, by going to the \mathbb{R}^2 Gaussian states and performing estimates depending on the index's distance from Dx_0 . The requirements on η, ε are intuitive, as the state $\Psi_{\mathbf{z}_0, \sigma, \mathbb{T}^2}$ is a Gaussian state with standard deviation of order $D^{-1/2}$ in position or momentum space, and so a state centered at $\mathbf{z}_0 + o(D^{-1/2})$ eventually overlaps strongly with one at \mathbf{z}_0 . The requirement on δ is for convenience so we can interchange the torus states with the \mathbb{R}^2 Gaussian states according to (S25).

This property is needed to handle the varying phases α_j, β_j in the DFT matrices; it is not required for the Balazs–Voros quantization with no phase factors.

B. Action on coherent states

We consider $\mathbf{z}_0 = (x_0, p_0)$ away from the discontinuities of the classical A -baker map; specifically for any $0 < \gamma < \frac{1}{2}$ and $0 < \delta < \frac{1}{2A}$, we consider

$$\mathcal{G}_{A, \delta, \gamma} = \left\{ (x_0, p_0) : \left| x_0 - \frac{k}{A} \right| > \delta \quad \forall k = 0, \dots, A, \text{ and } p_0 \in (\gamma, 1 - \gamma) \right\}.$$

This partitions $[0, 1]^2$ into A disjoint rectangles, $I_\ell \times \Gamma := \{x_0 \in (\frac{\ell}{A} + \delta, \frac{\ell+1}{A} - \delta)\} \times \{p_0 \in (\gamma, 1 - \gamma)\}$ for $\ell = 0, \dots, A-1$. For each rectangle $I_\ell \times \Gamma$, we consider a coherent state centered at some $\mathbf{z}_0 \in I_\ell \times \Gamma$, and compute its evolution under $\tilde{B}_A^{(\Pi)}$.

Suppose $\mathbf{z}_0 \in I_\ell \times \Gamma$, and let $j = \Pi(\ell)$. Since the coherent state $\Psi_{\mathbf{z}_0, \sigma, \mathbb{T}^2}$ is localized at \mathbf{z}_0 , it is small for coordinates away from I_ℓ , in particular, using (S25), then

$$\langle \xi | \Psi_{\mathbf{z}_0, \sigma, \mathbb{T}^2} \rangle = \frac{1}{\sqrt{D}} \mathcal{O}((\sigma D)^{1/4} e^{-\pi \sigma D \delta^2}), \quad \xi \notin \left[\ell \frac{D}{A}, (\ell+1) \frac{D}{A} - 1 \right], \quad (\text{S28})$$

since $|\frac{\xi}{D} - x_0| \geq \delta$. Thus the main contributions in $\tilde{B}_{A, \text{mix}}^{(\Pi)} |\Psi_{\mathbf{z}_0, \sigma, \mathbb{T}^2}\rangle$ will come from the ℓ th-block $\omega_\ell F_D^{\alpha_\ell, \beta_\ell}$ in $\tilde{B}_{A, \text{mix}}^{(\Pi)}$, since this block acts on the large elements of $|\Psi_{\mathbf{z}_0, \sigma, \mathbb{T}^2}\rangle$ which correspond to the indices $\xi \in [\ell \frac{D}{A}, (\ell+1) \frac{D}{A} - 1]$. This block has been permuted to the j th row block, and so we start with computing $\langle m | \tilde{B}_{A, \text{mix}}^{(\Pi)} |\Psi_{\mathbf{z}_0, \sigma, \mathbb{T}^2}\rangle$ for $m \in [j \frac{D}{A}, (j+1) \frac{D}{A} - 1]$. We are not concerned with phase factors that depend on $j, \ell, \alpha_\ell, \beta_\ell, D, A$, or \mathbf{z}_0 since these just become an overall phase factor, so we will accumulate them in a phase factor $e^{i\phi_{\Pi, \mathbf{z}_0}}$ which may change from line to line. We will have to keep track of phase factors depending on m . Using (S26), (S28), and Gaussian transformation properties, we compute,

$$\begin{aligned} \langle m | \tilde{B}_{A, \text{mix}}^{(\Pi)} |\Psi_{\mathbf{z}_0, \sigma, \mathbb{T}^2}\rangle &= \omega_j \sum_{\xi = \ell \frac{D}{A}}^{(\ell+1) \frac{D}{A} - 1} \langle m - jD/A | F_D^{\alpha_\ell, \beta_\ell} | \xi - \ell D/A \rangle \langle \xi | \Psi_{\mathbf{z}_0, \sigma, \mathbb{T}^2} \rangle \\ &= e^{i\phi_{\Pi, \mathbf{z}_0}} e^{-2\pi i \beta_\ell \frac{A}{D} m} \sqrt{A} \sum_{\xi=0}^{D-1} \langle Am - jD | F_D | \xi \rangle e^{-2\pi i \alpha_\ell \xi \frac{A}{D}} \langle \xi | \Psi_{\mathbf{z}_0, \sigma, \mathbb{T}^2} \rangle + \mathcal{O}(\sqrt{A}(\sigma D)^{1/4} e^{-\pi D \sigma \delta^2}) \\ &= e^{i\phi_{\Pi, \mathbf{z}_0}} e^{-2\pi i \beta_\ell \frac{A}{D} m} \sqrt{A} \langle Am - jD | \Psi_{F(x_0, p_0 - \alpha_\ell A/D), 1/\sigma, \mathbb{T}^2} \rangle + \mathcal{O}(\sqrt{A}(\sigma D)^{1/4} e^{-\pi D \sigma \delta^2}), \end{aligned} \quad (\text{S29})$$

where in the second line, we used (S28) to freely (at the cost of the error term $\mathcal{O}((\sigma D)^{1/4}e^{-\pi D\sigma\delta^2})$) add in the terms involving $\langle \xi | \Psi_{\mathbf{z}_0, \sigma, \mathbb{T}^2} \rangle$ for $\xi \notin [\frac{\ell D}{A}, \frac{(\ell+1)D}{A} - 1]$, and in the third line we used $e^{-2\pi i \alpha_\ell \xi \frac{A}{D}} \langle \xi | \Psi_{\mathbf{z}_0, \sigma, \mathbb{T}^2} \rangle = e^{-i\pi \alpha_\ell A x_0} \langle \xi | \Psi_{(x_0, p_0 - \alpha_\ell A/D), \sigma, \mathbb{T}^2} \rangle + \frac{1}{\sqrt{D}} \mathcal{O}((\sigma D)^{1/4} e^{-\pi \sigma D \delta^2})$ as well as the DFT action on the torus states.

By Gaussian state transformation properties, for $\mathbf{z} = (x_1, p_1)$,

$$\sqrt{A} \Psi_{F\mathbf{z}, 1/\sigma}(Ax - j) = \Psi_{((p_1+j)/A, -(Ax_1-\ell), A^2/\sigma)}(x) e^{i\pi D\ell(p_1+j)/A} e^{-\pi i D j x_1} e^{-2\pi i D \ell x}.$$

Then taking $x = m/D$ and D large enough so $\gamma - A/D \geq \gamma/2$ (so that $p_0 - \alpha_\ell A/D \in (\gamma/2, 1 - \gamma/2)$ and $\frac{p_0+j}{A} - \frac{\alpha_\ell}{D} \in (\frac{\gamma}{2A}, 1 - \frac{\gamma}{2A})$), then

$$\sqrt{A} \langle Am - jD | \Psi_{F(x_0, p_0 - \alpha_\ell A/D), 1/\sigma, \mathbb{T}^2} \rangle = \langle m | \Psi_{(\frac{p_0+j}{A} - \frac{\alpha_\ell}{D}, -(Ax_0-\ell), A^2/\sigma, \mathbb{T}^2)} e^{i\phi_{\Pi, \mathbf{z}_0}} + \mathcal{O}(\sigma^{-1/4} e^{-\pi D \gamma^2 / (4\sigma)}).$$

Using this in (S29) and taking into account the phase factor $e^{-2\pi i \frac{\beta_\ell A}{D} m}$, we obtain, for $m \in [j \frac{D}{A}, (j+1) \frac{D}{A} - 1]$,

$$\langle m | \tilde{B}_{A, \text{mix}}^{(\Pi)} | \Psi_{\mathbf{z}_0, \sigma, \mathbb{T}^2} \rangle = e^{i\phi_{\Pi, \mathbf{z}_0}} \langle m | \Psi_{(\frac{p_0+j}{A} - \frac{\alpha_\ell}{D}, -(Ax_0-\ell) - \frac{\beta_\ell A}{D}, A^2/\sigma, \mathbb{T}^2)} \rangle + \mathcal{O}(\max(\sigma, 1/\sigma)^{1/4} D^{1/2} e^{-\pi D \theta}), \quad (\text{S30})$$

where $\theta := \max(\sigma \delta^2, \gamma^2 / (4\sigma))$.

The same estimate holds for $m \notin [j \frac{D}{A}, (j+1) \frac{D}{A} - 1]$, essentially because everything on the right side of (S30) is just $\mathcal{O}(\max(\sigma, 1/\sigma)^{1/4} D^{1/2} e^{-\pi D \theta})$ as $|\frac{m}{D} - \frac{p_0+j}{A}| \geq \gamma/A$, and also so is the equivalent of the first line of (S29) by (S28). Then adding a factor \sqrt{D} to go to the euclidean norm, we obtain,

$$\left\| \tilde{B}_{A, \text{mix}}^{(\Pi)} \Psi_{(x_0, p_0), \sigma, \mathbb{T}^2} - e^{i\phi_{\Pi, \mathbf{z}_0}} \Psi_{(\frac{p_0+j}{A} - \frac{\alpha_\ell}{D}, -(Ax_0-\ell) - \frac{\beta_\ell A}{D}, A^2/\sigma, \mathbb{T}^2)} \right\| = \mathcal{O}(\max(\sigma, 1/\sigma)^{1/4} D e^{-\pi D \theta}).$$

Since the inverse DFT matrix F_D^{-1} is unitary, then also

$$\left\| \tilde{B}_A^{(\Pi)} \Psi_{(x_0, p_0), \sigma, \mathbb{T}^2} - e^{i\phi_{\Pi, \mathbf{z}_0}} \Psi_{(Ax_0-\ell + \frac{\beta_\ell A}{D}, \frac{p_0+j}{A} - \frac{\alpha_\ell}{D}, \sigma/A^2, \mathbb{T}^2)} \right\| = \mathcal{O}(\max(\sigma, 1/\sigma)^{1/4} D e^{-\pi D \theta}), \quad (\text{S31})$$

for $\theta = \max(\sigma \delta^2, \gamma^2 / (4\sigma))$. The above bound is $o(1)$ if for example, $\sigma \sim c$, $\gamma \sim c$, $\delta \sim \frac{c}{A}$, and $A = o(D^{1/2} (\log D)^{-1/2})$. Finally, using (S27) with $\eta = \frac{\beta_\ell A}{D}$ and $\varepsilon = -\frac{\alpha_\ell}{D}$, yields,

$$\left\| \tilde{B}_A^{(\Pi)} \Psi_{(x_0, p_0), \sigma, \mathbb{T}^2} - e^{i\phi_{\Pi, \mathbf{z}_0}} \Psi_{(Ax_0-\ell, \frac{p_0+j}{A}, \sigma/A^2, \mathbb{T}^2)} \right\| = o(1), \quad \text{as } D \rightarrow \infty. \quad (\text{S32})$$